Fasting-Mimicking Diet Drives Antitumor Immunity against Colorectal Cancer by Reducing IgA-Producing Cells

Ziwen Zhong[1,2], Hao Zhang[1,2], Ke Nan[1,2], Jing Zhong[1,2], Qichao Wu[1,2], Lihong Lu[1,3], Ying Yue[1,2], Zhenyu Zhang[1,2], Miaomiao Guo[1,2], Zhiqiang Wang[4], Jie Xia[5], Yun Xing[4], Ying Fu[4], Baichao Yu[4], Wenchang Zhou[1,2], Xingfeng Sun[6], Yang Shen[1,2], Wankun Chen[1,2], Jie Zhang[1,2], Jin Zhang[7], Duan Ma[7], Yiwei Chu[4], Ronghua Liu[5], and Changhong Miao[1,2]

ABSTRACT

As a safe, feasible, and inexpensive dietary intervention, fasting-mimicking diet (FMD) exhibits excellent antitumor efficacy by regulating metabolism and boosting antitumor immunity. A better understanding of the specific mechanisms underlying the immunoregulatory functions of FMD could help improve and expand the clinical application of FMD-mediated immunotherapeutic strategies. In this study, we aimed to elucidate the role of metabolic reprogramming induced by FMD in activation of antitumor immunity against colorectal cancer. Single-cell RNA sequencing analysis of intratumoral immune cells revealed that tumor-infiltrating IgA$^+$ B cells were significantly reduced by FMD treatment, leading to the activation of antitumor immunity and tumor regression in murine colorectal cancer models. Mechanistically, FMD delayed tumor growth by repressing B-cell class switching to IgA. Therefore, FMD-induced reduction of IgA$^+$ B cells overcame the suppression of CD8$^+$ T cells. The immunoregulatory and antitumor effects of FMD intervention were reversed by IgA$^+$ B-cell transfer. Moreover, FMD boosted fatty acid oxidation (FAO) to trigger RUNX3 acetylation, thus inactivating C_α gene transcription and IgA class switching. IgA$^+$ B-cell expansion was also impeded in patients placed on FMD, while B-cell expression of carnitine palmitoyl transferase 1A (CPT1A), the rate-limiting enzyme of FAO, was increased. Furthermore, CPT1A expression was negatively correlated with both IgA$^+$ B cells and IgA secretion within colorectal cancer. Together, these results highlight that FMD holds great promise for treating colorectal cancer. Furthermore, the degree of IgA$^+$ B cell infiltration and FAO-associated metabolic status are potential biomarkers for evaluating FMD efficacy.

Significance: Metabolic reprogramming of B cells induced by fasting-mimicking diet suppresses IgA class switching and production to activate antitumor immunity and inhibit tumor growth.

See related commentary by Bush and Perry, p. 3493

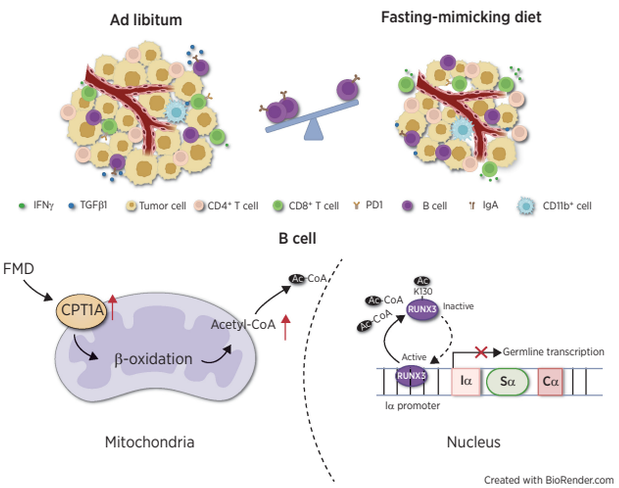

Introduction

Fasting-mimicking diet (FMD) is emerging as an effective dietary intervention with the potential to prolong life span in healthy people and boost antitumor immunity in patients with cancer. FMD refers to a medically designed fasting-like state that allows periodic consumption of a very-low-calorie and low-protein diet (1, 2). Compared with other dietary interventions like chronic caloric restriction or water-only

[1]Department of Anesthesiology, Zhongshan Hospital, Fudan University, Shanghai, China. [2]Shanghai Key Laboratory of Perioperative Stress and Protection, Shanghai, China. [3]Department of Anesthesiology, Department of Oncology, Fudan University Shanghai Cancer Center, Shanghai Medical College, Fudan University, Shanghai, China. [4]Department of Immunology, School of Basic Medical Sciences, and Shanghai Key Laboratory of Medical Epigenetics and Metabolism, Institutes of Biomedical Sciences, Fudan University, Shanghai, China. [5]Shanghai Fifth People's Hospital, and Shanghai Key Laboratory of Medical Epigenetics, Institutes of Biomedical Sciences, Fudan University, Shanghai, China. [6]Department of Anesthesiology, Obstetrics and Gynecology Hospital of Fudan University, Shanghai, China. [7]Key Laboratory of Metabolism and Molecular Medicine, Ministry of Education, Department of Biochemistry and Molecular Biology, Institute of Biomedical Sciences, Collaborative Innovation Center of Genetics and Development, School of Basic Medical Sciences, Fudan University, Shanghai, China.

Z. Zhong, H. Zhang, K. Nan, and J. Zhong contributed equally to this article.

Corresponding Authors: Changhong Miao, Department of Anesthesiology, Zhongshan Hospital, Fudan University, No.180 Fenglin Road, Shanghai 200032, China. E-mail: Miaochangh@hotmail.com; Ronghua Liu, Shanghai Fifth People's Hospital, and Shanghai Key Laboratory of Medical Epigenetics, Institutes of Biomedical Sciences, Fudan University, No.128 Ruili Road, Shanghai 200240, China. E-mail: ronghualiu@fudan.edu.cn

Cancer Res 2023;83:3529–43

doi: 10.1158/0008-5472.CAN-23-0323

fasting, FMD is safer, more feasible and inexpensive to patients with cancer (3).

Colorectal cancer is the third most common cancers worldwide, which is commonly accompanied by poor prognosis and therapy resistance (4). Therefore, identifying novel treatments that can be effective against colorectal cancer tumor growth is of crucial importance. A well-controlled effect of fasting or FMD on colorectal cancer has been shown in previous studies, which is associated with increased tumor cell autophagy, oxidative stress, and inhibition of aerobic glycolysis (5–7). Apart from controlling tumor cell growth by regulating metabolism of tumor cells, FMD is also regarded as a promising and powerful antitumor tool with its potential capability to remodel intratumor immune responses of colorectal cancer (2, 3, 8, 9). Both preclinical and clinical evidences have elucidated that FMD delays tumor progression and sensitizes a wide range of tumors to chemotherapy, potentially through facilitating antitumor immunity (1, 10–12). The combination of chemotherapy and FMD leads to a major delay in tumor progression in breast cancer and melanoma, which is accompanied by increased levels of common lymphoid progenitor cells and cytotoxic $CD8^+$ tumor-infiltrating lymphocytes in the bone marrow (13). Similarly, short-term fasting, a low-calorie, low-protein FMD, boosts antitumor responses by promoting tumor immunogenicity and decreasing local immunosuppression and selectively sensitizes cancer cells to chemotherapeutics (10). Moreover, a recent phase I clinical trial has shown that FMD reshapes both metabolism and antitumor immunity in patients suffering from cancer (3). However, changes in the overall immune pattern of colorectal cancer after FMD intervention are not completely understood.

Immunoglobulin A (IgA) producing cells provide the first line of immune protection at gut mucosal surfaces and also are recognized as an immunosuppressive or regulatory B cell subset due to their high expression of programmed death ligand-1 (PD-L1), IL10, TGFβ1, and even IgA (14–17). In this study, we display the immune cell atlas of murine colorectal cancer undergoing regular or FMD intervention by single-cell RNA sequencing (scRNA-seq) and found IgA^+ B cells were mostly decreased after FMD treatment. Moreover, we also show that FMD improves antitumor immunity by reducing IgA^+ B cells both in murine and human colorectal cancer. Besides, FMD abolished the inhibitory effect on $CD8^+$ T cells by reducing the class-switch recombination (CSR) of B cells to IgA, as FMD drove fatty acid oxidation (FAO) metabolism in B cells. These results elucidate that FMD can activate antitumor immunity against colorectal cancer by metabolic reprogramming, which provides evidence for tumor immunomodulatory capacity of FMD and its clinical significance in adjuvant therapy of colorectal cancer.

Materials and Methods

Subjects

ChiCTR2200062524 (http://www.chictr.org.cn/showproj.aspx?proj=174107) is a monocentric, open-label, prospective clinical trial aimed at evaluating the safety, feasibility, and metabolic and immunomodulatory effects of FMD in patients with colorectal cancer. Twenty-two participants were recruited from Zhongshan Hospital based on the established inclusion and exclusion criteria (Supplementary Tables S1 and S2). The main clinical characteristics of patients are summarized in Supplementary Table S3. All participants signed informed consent forms and were randomized in a 1:1 ratio to undergo FMD or a regular diet for 3 d before surgery. This clinical study was approved by the Ethics Committee of Zhongshan Hospital, Fudan University (Approval No.: B2020–063; ref. 2), in accordance with the Helsinki Declaration of 1975 as revised in 1983 (IRB no. 32378).

Human diet

The human FMD is a calorie-restricted, low-carbohydrate, and low-protein diet program that aims to achieve fasting-like effects, provides micronutrient nourishment and minimizes the burden of fasting (3, 8). It comprises tea, broths, steamed eggs, virgin olive oil, tofu pudding, milk and whole grain bread (Supplementary Fig. S1; Supplementary Tables S4 and S5). The calorie content declined from day 1 (∼600 kcal), to days 2 to 3 (∼300 kcal). Moreover, the carbohydrates/proteins/fats composition was approximately 55% to 58%/22% to 25%/15% to 20% on the first day and 35% to 40%/30% to 33%/30% to 33% on the other subsequent 2 days. The patients were allowed to eat the diet components at any time on the designated day. Participants in the control group were instructed to maintain their weight throughout the trial and remain on their usual diet.

Animals

IgA-deficient ($Iga^{-/-}$) mice were constructed by deleting the *Igha* gene, which were obtained from the Department of Immunology at Fudan University (Shanghai, China). All mice used had a C57BL/6 genetic background and were housed under specific pathogen-free conditions at the animal facility at Fudan University. Animal experiments were approved by the Institutional Animal Care and Use Committee of Fudan University (Permit Number: 202011009S). All animal experiments complied with the National Institute of Health's Guide for the Care and Use of Laboratory Animals (NIH Publications No. 8023, revised in 1978). The details and results of genotyping are shown in Supplementary Table S6.

Orthotopic mouse colorectal cancer model

Male mice (6–8 weeks old) were anesthetized with 2% pentobarbital and were fixed on a SMZ-168 stereomicroscope (Motic Co.). Subsequently, the anal canal was gently dilated using blunt forceps to expose the distal anal and rectal mucosa, which was performed as previously described (18, 19). A sterile 30-gauge removable needle on a 50 μL Hamilton Microliter Syringe (Hamilton Co.) was used for injections of MC38 cells (1×10^6 MC38 at a volume of 10 μL) into the submucosa. Transmural injection was avoided to prevent the establishment of a pelvic cavity tumor model. After the injection, the mice were observed for 1 hour to ensure uncomplicated recovery.

Azoxymethane plus dextran sodium sulfate mouse colorectal cancer model

Mice were intraperitoneally injected with 10 mg/kg body weight azoxymethane (AOM; Sigma), as described previously (20). One week after AOM administration, the mice were fed three dextran sodium sulfate (DSS; molecular weight 36,000 to 50,000, MP Biomedicals) cycles. The DSS cycles were separated by 2.5% (w/v) DSS for 1 week and 2 weeks of regular drinking water.

Rodent diets and treatments

Mice were kept on irradiated AIN-93G purified rodent chow (Dyets). This diet contained 4 kcal/g of gross energy with calories supplied by proteins, carbohydrates, and fat in a percentage ratio of 20:64:16. Food was provided *ad libitum*. Mice in the control group were fed with AIN-93G during the whole procedure. Our FMD diet is based on a nutritional screen that identifies ingredients allowing

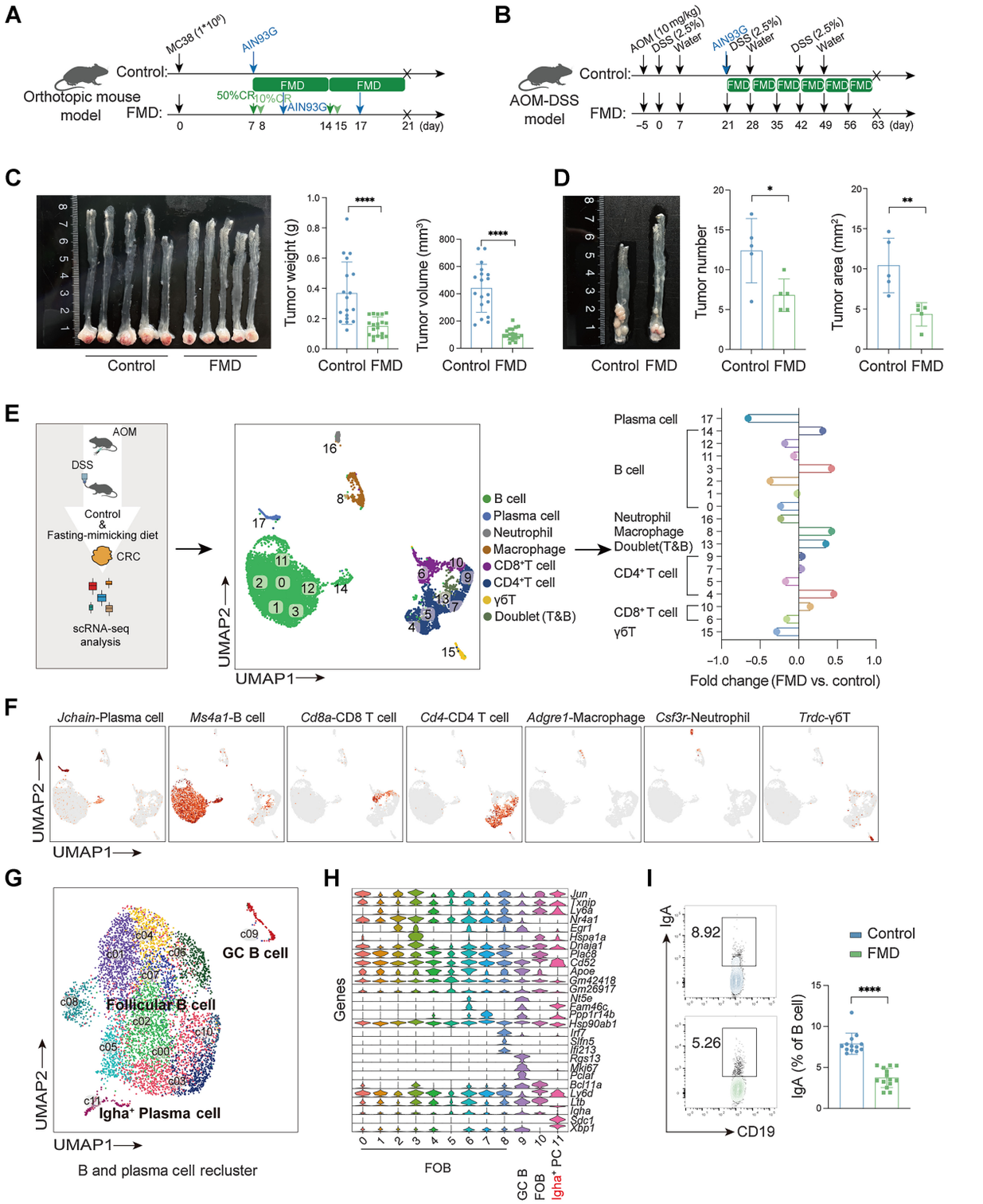

Figure 1.

FMD inhibits colorectal cancer progress with the reduction of IgA$^+$ cells. **A** and **B,** Schematic diagram of orthotopic mouse models and AOM plus DSS mouse models. **A,** Eight-week-old male C57 mice were grafted with MC38 cells and subjected to AIN93G or multiple cycles of FMD. **B,** Experimental design for the AOM plus DSS-induced mouse colon cancer model with AIN93G or multiple cycles of FMD. **C,** Tumor volume and tumor weight prior to euthanasia were observed for each treatment. **D,** Tumor number and tumor area prior to euthanasia were observed for each treatment. **E–I,** CD45$^+$ immune cells were sorted using FC from mouse colon containing most neoplasia tissues of colorectal cancer models with AIN93G and FMD treatment. **E,** Single-cell sequencing was performed in a pool of four mice per group. The immune landscape of colorectal cancer is displayed by UMAP plot and differentially clusters were identified through fold change filtering. **F,** FeaturePlots of classical immune cell markers. **G,** Recluster of bulk B cell and PC. **H,** Violin plots of signature genes in each B cluster. **I,** Expression of IgA$^+$ B cells was verified using FC. The data in **B**, **D**, and **I** are presented as means± SEM. *P* values were determined by a two-tailed unpaired Student *t* test. *, $P < 0.05$; **, $P < 0.01$; ****, $P < 0.0001$. CRC, colorectal cancer; FOB, follicular B cell.

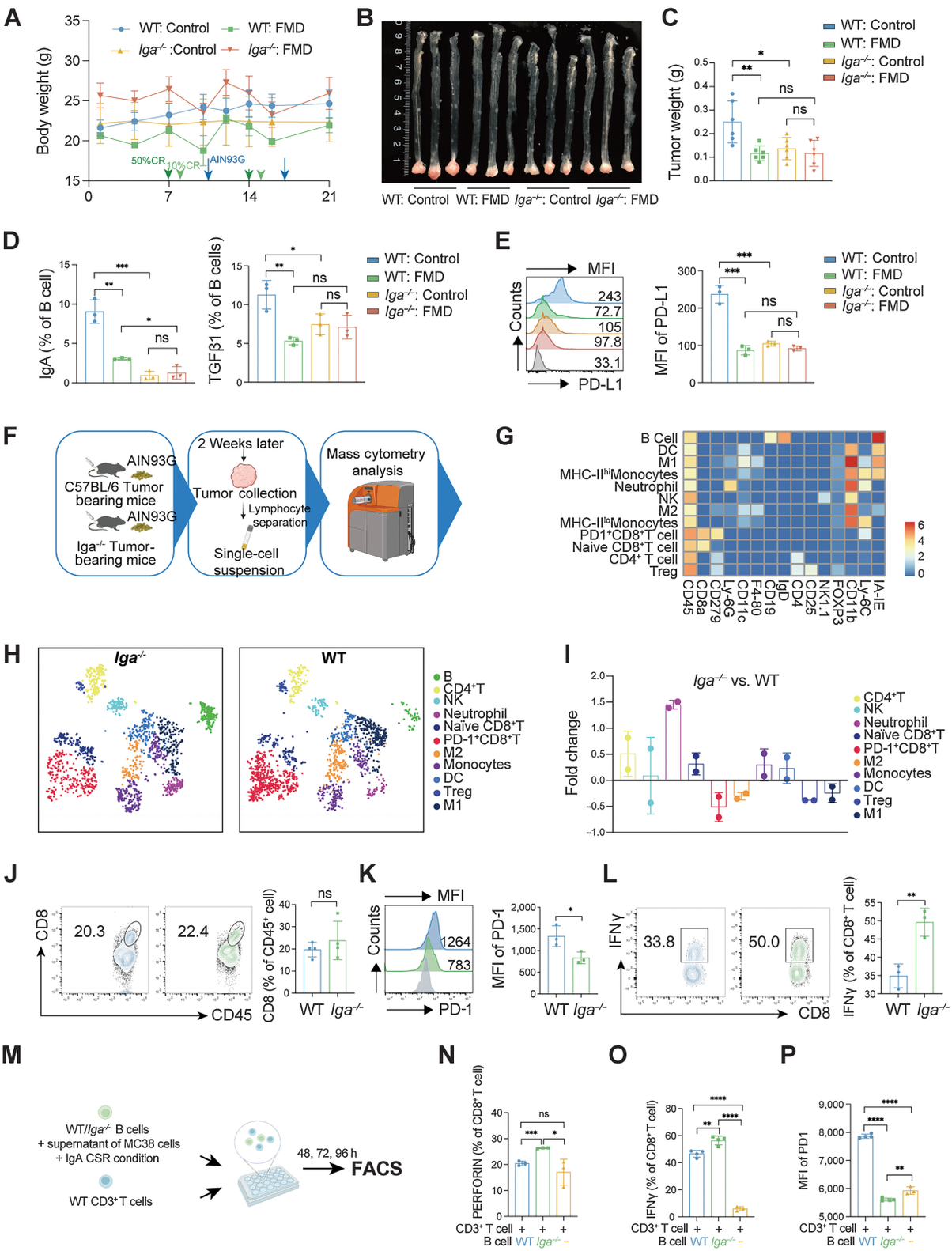
A
Body weight (g)
WT: Control
WT: FMD
Iga−/− :Control
Iga−/−: FMD
50%CR
10%CR
AIN93G
B
WT: Control WT: FMD Iga−/−: Control Iga−/−: FMD
C
Tumor weight (g)
WT: Control
WT: FMD
Iga−/−: Control
Iga−/−: FMD
D
IgA (% of B cell)
TGFβ1 (% of B cells)
E
MFI
Counts
243
72.7
105
97.8
33.1
PD-L1
MFI of PD-L1
F
AIN93G
C57BL/6 Tumor bearing mice
Iga−/− Tumor-bearing mice
2 Weeks later
Tumor collection
Lymphocyte separation
Single-cell suspension
Mass cytometry analysis
G
B Cell
DC
M1
MHC-IIhiMonocytes
Neutrophil
NK
M2
MHC-IIloMonocytes
PD1+CD8+T cell
Naive CD8+T cell
CD4+ T cell
Treg
CD45
CD8a
CD279
Ly-6G
CD11c
F4-80
CD19
IgD
CD4
CD25
NK1.1
FOXP3
CD11b
Ly-6C
IA-IE
H
Iga−/−
WT
B
CD4+T
NK
Neutrophil
Naïve CD8+T
PD-1+CD8+T
M2
Monocytes
DC
Treg
M1
I
Iga−/− vs. WT
Fold change
J
CD8
20.3
22.4
CD45
CD8 (% of CD45+ cell)
WT Iga−/−
K
MFI
Counts
1264
783
PD-1
MFI of PD-1
L
IFNγ
33.8
50.0
CD8
IFNγ (% of CD8+T cell)
M
WT/Iga−/− B cells
+ supernatant of MC38 cells
+ IgA CSR condition
WT CD3+ T cells
48, 72, 96 h
FACS
N
PERFORIN (% of CD8+T cell)
O
IFNγ (% of CD8+T cell)
P
MFI of PD1
CD3+ T cell
B cell
WT
Iga−/−

high nourishment during periods of low-calorie consumption. The FMD consisted of a day 1 diet, day 2–3 diet, and day 4 to 7 diet, as described previously (7). The 50% calorie restriction (CR) diet was fed on day 1 (mice were provided 50% of AIN-93G intake; 0.11 kJ/g carbohydrates, 1.17 kJ/g protein, and 0.53 kJ/g fat). The 10% CR diet was fed on days 2–3 (provided 10% of AIN-93G intake; 0.34 kJ/g carbohydrates, 0.01 kJ/g protein). AIN-93G was administered on days 4–7.

All orthotopic colorectal cancer mice were randomly allocated to the Control group or FMD group using random number table method. For the orthotopic mouse colorectal cancer model, mice in the FMD group were first placed on a 7 d AIN-93G diet and then two FMD cycles after mouse modeling. For the AOM plus DSS mouse colorectal cancer model, the mice were fed six FMD cycles after the first DSS cycle. Mouse weight was monitored every 2 days, and weight loss did not exceed 20%.

To determine which individual components (proteins, carbohydrates, and fats) of the diets may drive tumor progression, we then conducted rescue experiments according to the calorie difference between the AIN-93G, 50% CR, and 10% CR diets in terms of each component. The FMD + sugar group was provided with a day 1 diet plus 43.64 g/kg body weight sucrose supplementation and day 2–3 diet plus 62.73 g/kg body weight sucrose supplementation. The FMD + protein group was provided with day 1 diet plus 20 g/kg body weight casein supplementation and day 2 to 3 diet plus 45.46 g/kg body weight casein supplementation. The FMD + fat group was provided with day 1 diet plus 1.82 g/kg body weight soybean oil supplementation and day 2 to 3 diet plus 8.18 g/kg body weight soybean oil supplementation.

Cell lines and culture conditions

MC38 (RRID: CVCL_B288), HEK293T (RRID: CVCL_0045), and CHO (RRID: CVCL_1977) cell lines were obtained from ATCC. All cells were cultured in DMEM supplemented with 10% FBS and 1% penicillin/streptomycin. Cells were grown at 37°C in a 5% CO_2 setting. For FMD-like condition experiments, cells were grown in DMEM medium without glucose supplemented with 0.5 g/L glucose and 1% FBS.

B-cell culture *in vitro* and IgA class-switching assay

B cells were purified from the spleen of mice using a B Cell Isolation Kit (STEMCELL) and cultured in at least three replicate wells of 48-well plates (4×10^5 cells per well). Purified B cells were cultured for 5 days in the presence of MC38 supernatants and IgA class switching condition [LPS (5 μg/mL), TGFβ (5 ng/mL), BAFF (20 ng/mL), anti-CD40 (2 μg/mL), and anti-IgM (2 μg/mL)]. For FMD-like condition experiments, 5 days were divided into seven periods, each containing 17 hours. B cells were cultured in RPMI1640 medium without glucose supplemented with 1.0 g/L glucose and 5% FBS for the first 17 hours, and were then replaced with glucose-free RPMI1640 medium supplemented with 0.2 g/L glucose and 1% FBS in the second and third 17 hours. For the remaining four periods, B cells were cultured in a normal RPMI1640 medium supplemented with 10% FBS, in accordance with the FMD regimen *in vivo*.

Coculture of B and T cells

B cells were purified from the spleens of wild-type (WT) and *Iga*$^{-/-}$ mice using a B Cell Isolation Kit (STEMCELL). CD3$^+$ T cells were isolated from the spleens of WT mice using a T Cell Isolation Kit (STEMCELL). WT and *Iga*$^{-/-}$ B cells were pretreated with MC38 supernatants and IgA class switching condition (LPS (5 μg/mL), TGFβ (5 ng/mL), BAFF (20 ng/mL), anti-CD40 (2 μg/mL), and anti-IgM (2 μg/mL)) for 5 days. Then purified WT CD3$^+$ T cells were cultured either alone or with B cells in 48-well plates for 48 hours, 72 hours and 96 hours (B:T ratio = 1:3).

Statistics analysis

Data were analyzed using GraphPad Prism version 9.2.0 for macOS, GraphPad Software, San Diego, California, www.graphpad.com and are presented as the mean ± SEM. Statistical significance was determined using a two-tailed Student *t* test and one-way or two-way analysis of variance. The cumulative survival time was calculated using the Kaplan–Meier method and analyzed using the log-rank test. Pearson correlation coefficient was used to analyze the correlations between the groups. Statistical significance was set at $P < 0.05$. *P* values are indicated as follows: ns, not significant; *, $P < 0.05$; **, $P < 0.01$; ***, $P < 0.001$; ****, $P < 0.0001$.

Data availability

The single-cell sequencing data generated in this study are publicly available in Gene Expression Omnibus at GSE212911. Other sources of protein and nucleic acid sequences are indicated in the manuscript and are available from the corresponding author on request. For The Cancer Genome Atlas (TCGA) cohort, the data generated in this study are publicly available in TCGA–colon adenocarcinoma (COAD) dataset with 450 tumor samples, and were downloaded from UCSC XENA (https://xena.ucsc.edu/). Further information on materials and methods is included in the Supplementary Materials and Methods. All the primers and antibodies used are listed in Supplementary Tables S7 to S9. All other raw data are available upon request from the corresponding author.

Figure 2.

FMD-induced tumor regression is disrupted by IgA$^+$ B cells. **A–E,** Orthotopic mouse model was constructed on *Iga* deletion (*Iga*$^{-/-}$) and WT mice, followed by AIN93G or multiple cycles of FMD treatment. **A,** Changes in body weight during the experiment. **B–E,** Tumor development and tumor weight were observed (**B** and **C**), followed by analyses of intratumoral IgA$^+$ B cells, TGFβ1, and PD-L1 in B cells (**D** and **E**). **F,** Single-cell suspension was isolated from the orthotopic mouse colorectal cancer model in *Iga*$^{-/-}$ and WT mice, followed by CyTOF analysis. **G,** Heat map displaying normalized marker expression of each immune cluster. **H,** The distributions of tumor-infiltrating leukocytes from WT ($n = 2$, pool of two mice per sample) versus *Iga*$^{-/-}$ ($n = 2$, pool of two mice per sample) mice, including tumor-infiltrating lymphocytes (T and B cells), monocytes, neutrophils, NK cells, and macrophages, are presented as two-dimensional t-SNE plots. **I,** The differentially clusters were identified through fold change filtering. **J–L**, The changes in CD8$^+$ T cells were further confirmed using FC, including CD8, PD-1, and IFNγ. **M,** WT and *Iga*$^{-/-}$ B cells were pretreated with MC38 supernatants and IgA class switching condition [LPS (5 μg/mL), TGFβ (5 ng/mL), BAFF (20 ng/mL), anti-CD40 (2 μg/mL), and anti-IgM (2 μg/mL)] for 5 days. Then purified WT CD3$^+$ T cells were cultured either alone or with B cells in 48-well plates for 48 hours, 72 hours, and 96 hours (B:T ratio = 1:3). **N–P,** IFNγ, PERFORIN, and PD-1 expression of CD8$^+$ T cells were measured 72 hours later. Data are shown as means ± SEM. ns, not significant; *, $P < 0.05$; **, $P < 0.01$; ***, $P < 0.001$; ****, $P < 0.0001$. BAFF, B cell-activating factor; CyTOF, cytometry by time of flight; MACS, magnetic activated cell sorting; MFI, mean fluorescence intensity; t-SNE, t-distributed stochastic neighbor embedding. (**F** and **M,** Created with BioRender.com.)

Results

FMD inhibits colorectal cancer progress with the reduction of IgA$^+$ cells

To reveal the antitumor effect of FMD in colorectal cancer, both MC38-induced orthotopic and AOM plus DSS mouse colorectal cancer models were constructed, followed by regular or FMD treatment (**Fig. 1A** and **B**). The results showed that tumor progression was significantly repressed after FMD treatment in both colorectal cancer models (**Fig. 1C** and **D**) without significant body weight changes (Supplementary Fig. S2A). Next, CD45$^+$ cells were isolated from the tumor tissues of colorectal cancer mice induced by AOM plus DSS, and scRNA-seq was performed to reveal alterations in the colorectal cancer immune landscape following FMD treatment (**Fig. 1E**). Eighteen clusters of 10× genomic data were identified using graph-based clustering. The examinations of canonical marker genes revealed major cell populations, including B cell (*Ms4a1*), with the highest cell count, CD4 T cell (*Cd4*), CD8 T cell (*Cd8a*), neutrophil (*Csf3r*), macrophages (*Adgre1*), plasma cells (PC; *Jchain*), and ??T (*Trdc*; **Fig. 1E** and **F**), which were also confirmed using flow cytometry (FC; Supplementary Fig. S2B). Among these immune cell populations, the decrease of PC was pronounced in the FMD group compared with the control group (**Fig. 1E**). B, T cells were further partitioned through a second round of clustering analysis and yielded 12 and 11 clusters, respectively. Among B and PCs, B cells-c00–08, c10-*Ighm* and *Ighd*, representing follicular B cells, were found no difference in two groups. B cells-c09-*Mki67*, on behalf of germinal center (GC) B, were enriched in the FMD group. PCs-c11-*Igha*, corresponding to IgA$^+$ PCs were significantly decreased in the FMD group (**Fig. 1G** and **H**), which was confirmed using FC (**Fig. 1I**). Meanwhile, the analysis of T re-clustering showed an increased frequency of central memory T cells and a reduced percentage of exhausted CD8$^+$ T in the FMD group (Supplementary Fig. S2C–S2E). These results confirm that FMD delays colorectal cancer progression while being accompanied by changes in the immune landscape, in which IgA-producing cells are significantly reduced.

IgA$^+$ B cells antagonize the antitumor effect of FMD in colorectal cancer

To validate the role of IgA$^+$ B cells in colorectal cancer, orthotopic mouse colorectal cancer models in WT and *Iga*$^{-/-}$ mice were constructed and placed on an *ad libitum* diet or FMD cycles, respectively. The results showed that IgA ablation barely affected weight gain (**Fig. 2A**), whereas compared with the WT control group, tumor weight and size were smaller in the *Iga*$^{-/-}$-control group. TGFβ1 secretion and PD-L1 expression in B cells were greatly decreased in the *Iga*$^{-/-}$-control group, implying an immunosuppressive role of IgA$^+$ B cells in colorectal cancer (**Fig. 2B–E**). Moreover, there were no significant differences between the *Iga*$^{-/-}$-control and *Iga*$^{-/-}$-FMD groups. To further confirm that FMD affected colorectal cancer growth by inhibiting IgA$^+$ B cells, adoptive transfer of WT IgA$^-$ or WT IgA$^+$ B cells was performed on an *ad libitum* diet or FMD cycles in *Iga*$^{-/-}$ mice bearing MC38 colon tumor cells (Supplementary Fig. S3A). Significantly, compared with the adaptive transfer of IgA$^-$ B cells, the antitumor effect was reversed after the adaptive transfer of IgA$^+$ B cells in the FMD group, which suggests that IgA$^+$ B cells work as the target cells to antagonize the antitumor effect of FMD (Supplementary Fig. S3B–S3F).

To find potential immunosuppressive targets of IgA$^+$ B cells, the tumor-infiltrating immune profiles of colorectal cancer WT and *Iga*$^{-/-}$ mice were analyzed using CyTOF (**Fig. 2F–I**). Fifteen surface and intracellular immune markers were included in the analysis of immune cell lineages and functional molecules (**Fig. 2G**). Analysis of the CD45$^+$ cells revealed 11 distinct subsets, including tumor-infiltrating lymphocytes (T and B cells), monocytes, neutrophils, natural killer (NK) cells, and macrophages (**Fig. 2H**). Among them, neutrophil clusters obviously increased and programmed cell death protein 1 (PD-1)$^+$ CD8$^+$ T-cell clusters decreased in *Iga*$^{-/-}$ mice, all other clusters were changed slightly in *Iga*$^{-/-}$ mice compared with WT mice (**Fig. 2I**). The changes in CD8$^+$ T-cell subsets were further confirmed using FC (**Fig. 2J–L**). As results shown, the secretion of IFNγ was significantly enhanced, while PD-1 expression was markedly reduced in *Iga*$^{-/-}$ mice. To confirm the suppression of IgA$^+$ B cells on T cells (**Fig. 2M**), WT and *Iga*$^{-/-}$ B cells were cultured with tumor supernatants of MC38 respectively, in combination with IgA class switching condition for 5 days. Then the purified CD3$^+$ T cells were cultured alone or with these pretreated B cells (B:T ratio = 1:3) for 48 hours. Our results show that although there were no significant differences in proliferation (Supplementary Fig. S3G and S3H), CD8$^+$ T cells that were cocultured with *Iga*$^{-/-}$ B cells expressed more activation markers than those with WT B cells (**Fig. 2N** and **O**), but lower exhausted marker PD-1 (**Fig. 2P**). These *in vivo* and *in vitro* experiments indicate that the reduction of IgA$^+$ B cells relieves the inhibitory effect on CD8$^+$ T cells and contributes to the antitumor effect.

FMD hinders class switching of B cells to IgA

The aberrant production of IgA by FMD prompted us to evaluate its role in regulating IgA class switching. Previous studies have confirmed that the lamina propria and Peyer's patches (PP) are active in IgA class switching (21). On the basis of the current study, FMD reduced the amount of IgA in the lamina propria and PPs of MC38-induced orthotopic colorectal cancer mice (**Fig. 3A** and **B**). Moreover, although no significant differences were observed in serum, IgA production in the fecal supernatant and intestinal tumor homogenate was markedly decreased in the FMD group (**Fig. 3C**). Ig A class switching was initiated by the expression of IgA germline transcript (α-GLT) and required the activation-induced cytidine deaminase (AID). Then the expression of α-GLT, IgG1 germline transcript (γ-GLT), and AID (*Aicda*) in PPs were measured by quantitative qPCR (**Fig. 3D–F**). B cells in the FMD group showed a significant decrease in α-GLT and AID, while γ-GLT expression was not affected, which was also verified using FC (**Fig. 3G**). The role of FMD in regulating IgA class switching was further investigated with a well-characterized *in vitro* protocol (**Fig. 3H**; Supplementary Fig. S4A; ref. 22). FMD greatly repressed the induction of IgA$^+$ B cells *in vitro* (**Fig. 3I**). Furthermore, enzyme-linked immunospot (ELISPOT) assays and ELISA also confirmed that IgA secretion considerably decreased in FMD condition (**Fig. 3J** and **K**). To further prove that IgA class switching was affected by FMD, the expression of α-GLT and AID was detected. The results show that α-GLT and AID expression decreased in the FMD group, which was consistent with the results *in vivo* (**Fig. 3L**). Therefore, these findings emphasize that FMD negatively regulate class switching to IgA, leading to the reduction of IgA$^+$ cells in colorectal cancer following FMD treatment.

FMD evokes FAO program to inhibit IgA class switching

To gain insight into the metabolic pathway by which FMD regulates IgA class switching, glucose, protein, and fat were supplemented in FMD in orthotopic colorectal cancer mice, and the tumor burden and IgA cell levels were examined. The results showed that fat

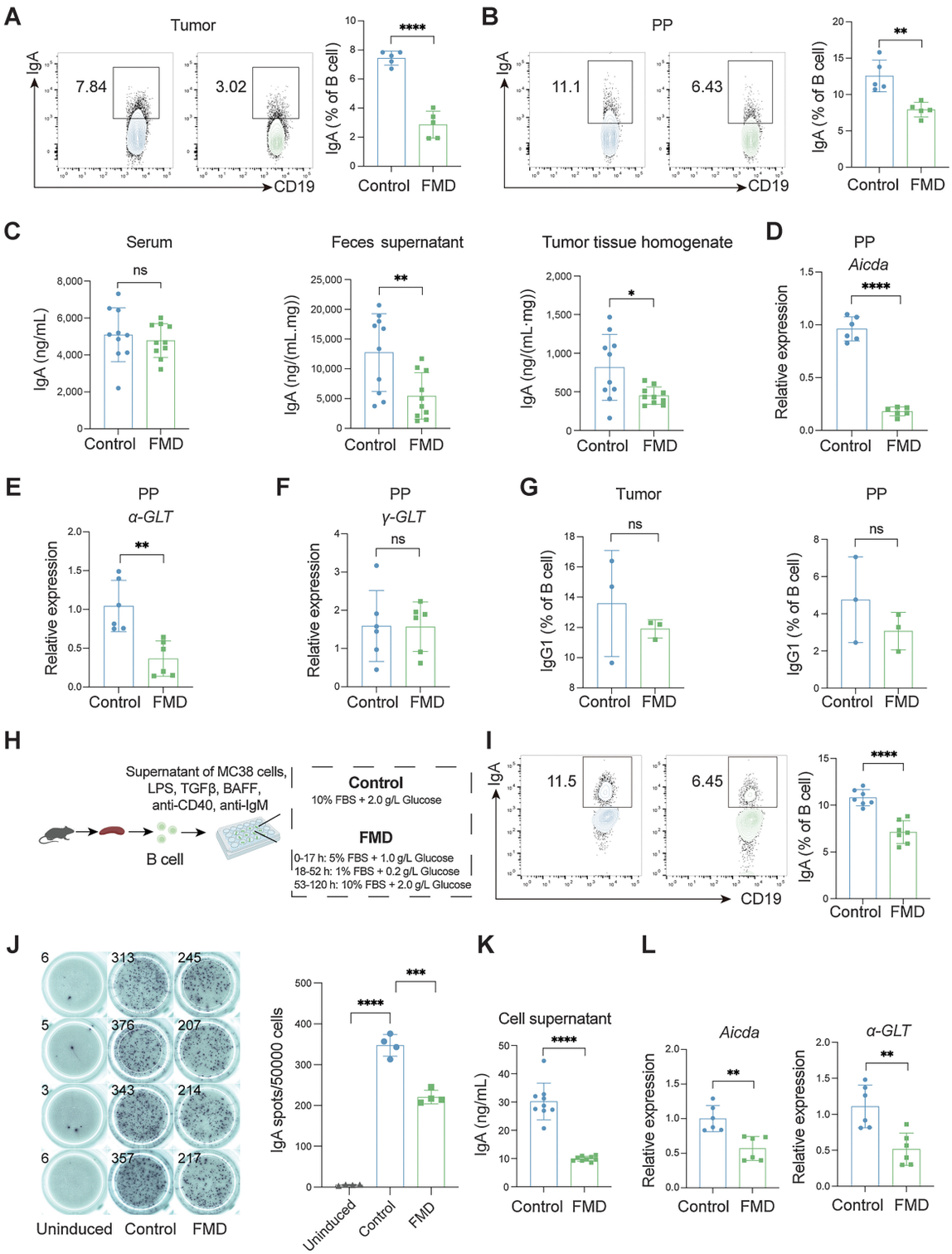

Figure 3.

FMD negatively regulates B-cell class switching to IgA *in vivo* and *in vitro*. **A** and **B,** The proportions of IgA$^+$ cells in tumor and PP of orthotopic colorectal cancer mice placed on an AIN93G or an FMD, assessed with FC. **C,** Scatter bar plot of IgA from serum, feces supernatant, tumor tissue homogenate of mice placed on an AIN93G or FMD as determined using ELISA. **D–F,** Quantitative PCR analysis of mRNA related to *Aicda*, α-GLT, and γ-GLT in PPs. **G,** Representative FC plots and graph representing the proportions of IgG1$^+$ B cells in tumor and PP. **H,** A schematic exhibits methods of FMD and inducing IgA class switching *in vitro*. Splenic B cells cultured for 5 days in the presence of MC38 supernatants and IgA class switching condition [LPS (5 μg/mL), TGFβ (5 ng/mL), BAFF (20 ng/mL), anti-CD40 (2 μg/mL), and anti-IgM (2 μg/mL)]. **I–K,** The expression of IgA was quantified using FC (**I**), ELISPOT assay (**J**), and ELISA (**K**). **L,** Quantitative PCR analysis of mRNA related to *Aicda* and α-GLT in splenic B cells cultured for 5 days under the condition of IgA class switching. Data are shown as means± SEM. ns, not significant; *, $P < 0.05$; **, $P < 0.01$; ***, $P < 0.001$; ****, $P < 0.0001$. ELISPOT, enzyme-linked immunospot. (**H,** Created with BioRender.com.)

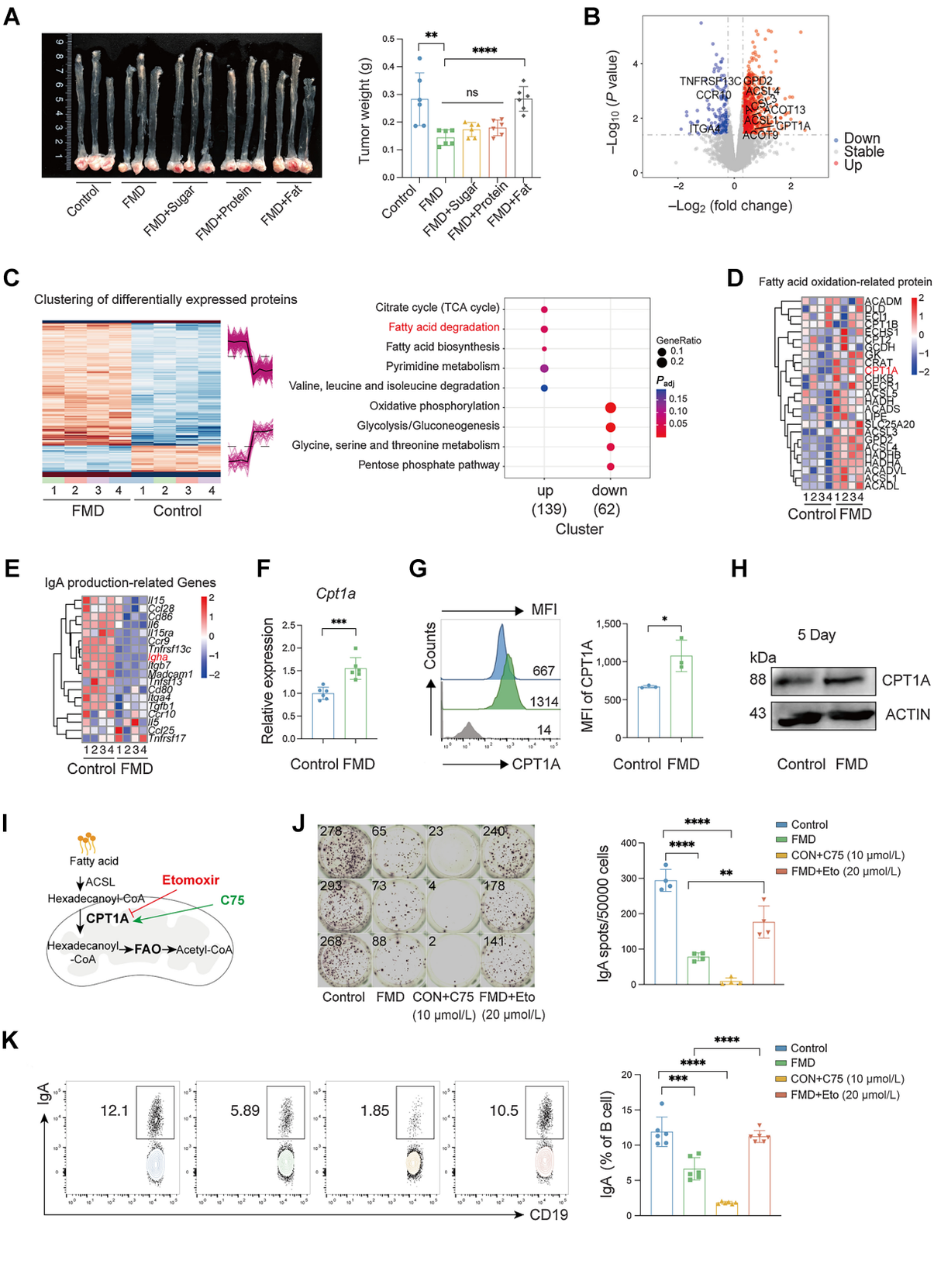
A
Control
FMD
FMD+Sugar
FMD+Protein
FMD+Fat
Tumor weight (g)
**
****
ns
B
–Log10 (P value)
–Log2 (fold change)
TNFRSF13C
CCR10
ITGA4
GPD2
ACSL4
ACSL3
ACOT13
ACSL1
CPT1A
ACOT9
Down
Stable
Up
C
Clustering of differentially expressed proteins
FMD
Control
Citrate cycle (TCA cycle)
Fatty acid degradation
Fatty acid biosynthesis
Pyrimidine metabolism
Valine, leucine and isoleucine degradation
Oxidative phosphorylation
Glycolysis/Gluconeogenesis
Glycine, serine and threonine metabolism
Pentose phosphate pathway
GeneRatio
Padj
up (139)
down (62)
Cluster
D
Fatty acid oxidation-related protein
Control FMD
E
IgA production-related Genes
Control FMD
F
Cpt1a
Relative expression
Control FMD
G
MFI
Counts
667
1314
14
CPT1A
MFI of CPT1A
Control FMD
H
5 Day
kDa
88
43
CPT1A
ACTIN
Control FMD
I
Fatty acid
ACSL
Hexadecanoyl-CoA
CPT1A
Etomoxir
C75
Hexadecanoyl -CoA
FAO
Acetyl-CoA
J
278
65
23
240
293
73
4
178
268
88
2
141
Control
FMD
CON+C75 (10 μmol/L)
FMD+Eto (20 μmol/L)
IgA spots/50000 cells
K
IgA
CD19
12.1
5.89
1.85
10.5
IgA (% of B cell)

supplementation reversed the antitumor effect of FMD, accompanied by an increase in IgA, implying a role of lipid metabolism in FMD controlling colorectal cancer and IgA class switching (**Fig. 4A**; Supplementary Fig. S4B). Furthermore, in our comparative proteome analysis of B cells cultured for 5 days *in vitro* under FMD or control conditions, 139 upregulated proteins and 62 downregulated proteins were identified (**Fig. 4B** and **C**). Functional enrichment analysis showed that FAO metabolic pathways were rapidly enriched within 5 days of FMD. The elevation of FAO-related proteins was accompanied by the downregulation of IgA production-related molecules in the FMD group compared with that in the control group (**Fig. 4D** and **E**), while the protein expression of other significantly different metabolic pathways was not as remarkable as that of FAO-related proteins (Supplementary Fig. S4C). Consequently, combined with the results from *in vivo* experiments, we hypothesized that FMD regulates FAO to suppress IgA class switching.

Next, the expression of carnitine palmitoyl transferase 1A (CPT1A), the rate-limiting enzyme of FAO, was examined in B cells cultured for 5 days *in vitro* under FMD or control condition. FMD markedly increased both mRNA and protein levels of CPT1A in B cells (**Fig. 4F–H**). Subsequently, we confirmed the role of FAO in regulating IgA class switching both *in vitro* and *in vivo*. *In vitro*, the effects of FMD on reducing IgA were reversed after the addition of etomoxir, an irreversible CPT1A inhibitor, to B cells under FMD conditions. IgA production was significantly depressed in B cells when C75, a CPT1A activator, was added to the control medium (**Fig. 4I–K**; Supplementary Fig. S4D and S4E). Moreover, intraperitoneal injection of etomoxir into tumor bearing C57BL/6 mice significantly reversed the antitumor effect of FMD and its inhibitory effect on IgA^+ B cells, while intraperitoneal injection of C75 markedly suppressed tumor growth and IgA production (Supplementary Fig. S5A–S5E). In addition, the adoptive transfer of B cells pretreated with etomoxir or C75 for 5 days into tumor bearing $Iga^{-/-}$ mice also affected the growth of tumors and the production of IgA^+ B cells, which was consistent with the previous results (Supplementary Fig. S5F–S5J). Indeed, these data illustrate that FMD inhibits IgA class switching in an FAO-dependent manner.

FAO-dependent acetylation is responsible for hindering IgA class switching

As a multistep process, FAO includes the degradation of fatty acids by sequential removal of 2-carbon units from the acyl chain to produce Acetyl-coenzyme A (acetyl-CoA; **Fig. 4I**). To determine how FAO diminished IgA class switching, proteomic quantification of lysine (Lys) acetylation in B cells subjected to FMD was performed. In the 1962 Lys acetylation sites from FMD and control B cells, the acetylation of RUNX3 increased in the FMD group and K130 was the main RUNX3 acetylation site (**Fig. 5A**). Moreover, Western blotting and immunoprecipitation (IP) showed that FMDs elevated the acetylation of RUNX3 without affecting its protein expression in B cells, consistent with the proteomic quantification of Lys acetylation (**Fig. 5B** and **C**). Next, CHO cells were transfected with WT RUNX3 and an acetylation-defective mutant, RUNX3-K130R. Transfection efficiency is shown in **Fig. 5D**. We found that FMD treatment increased the acetylation of RUNX3, but no significant difference was found when K130 was mutated to arginine (K130R) or when etomoxir was added to the medium, indicating that FMD elevates RUNX3 acetylation in a FAO-dependent manner (**Fig. 5E**). To confirm whether acetylation of RUNX3 is involved in IgA class switching, luciferase assays demonstrated that RUNX3 promoted the transcription of *Igha*, and its transcriptional activity was inhibited under FMD conditions. However, the transcriptional activity of the acetylation-defective mutant RUNX3 did not decrease under FMD conditions (**Fig. 5F**). The transcriptional regulation of *Igha* by RUNX3 under FMD treatment was confirmed by silencing the RUNX3 gene in B cells (**Fig. 5G–I**). These findings suggest that FAO-triggered RUNX3 acetylation is responsible for FMD hindering IgA class switching (**Fig. 5J**).

FMD treatment accelerates FAO and reduces IgA^+ B cells in patients with colorectal cancer

To determine the potential clinical significance of IgA-expressing B cells in colorectal cancer, the expression of IgA CSR-related and FAO-related genes in patients with colorectal cancer was analyzed using TCGA dataset. Interestingly, the results implied that the higher the ratio of FAO-related to IgA CSR-related genes, the higher the survival rate of patients with colorectal cancer (Supplementary Fig. S6A). Moreover, patients with low expression of IgA CSR-related genes and high expression of FAO-related genes exhibited the best overall survival compared with the other groups (**Fig. 6A**). Further results from FC and immunofluorescence staining showed that IgA expression in B cells was negatively correlated with CPT1A expression (**Fig. 6B** and **C**; Supplementary Fig. S6B–S6D).

Next, 22 patients with colorectal cancer were recruited into an FMD clinical trial (ChiCTR2200062524). Of these, 2 patients were excluded for inability to tolerate starvation (Supplementary Table S1). Finally, 10 patients underwent FMD and 10 patients underwent a regular diet for 3 d before surgery (Supplementary Fig. S1; Tables 2–5). Blood, feces, and tumor tissue samples were collected during the procedure (**Fig. 6D**). The common adverse events among the 10 patients who completed FMD were fatigue (10%) and dizziness (10%; Supplementary Table S10). The changes in the colorectal cancer immune cell atlas following FMD treatment were detected using FC. As the results shown, the total $CD4^+$ T, $CD8^+$ T, B, and $CD11b^+$ cell subsets did not significantly change, whereas FMD notably increased the percentage of

Figure 4.

FMD elicits a FAO program to inhibit IgA class switching. **A,** Glucose, protein, and fat were supplemented respectively into orthotopic colorectal cancer mice undergoing FMD, and followed by an examination of tumor burden. **B–D,** B cells were isolated from the spleen of WT mice and treated with control or FMD medium for 5 days in the presence of MC38 supernatants and IgA class switching condition. Protein expression in B cells was analyzed using mass spectrometry. **B,** Volcano plot of proteome analysis showing the differential proteins between the control and FMD groups. **C,** 139 upregulated proteins and 62 downregulated proteins were identified, and the fatty acid degradation metabolic pathway was markedly activated in the FMD group. **D** and **E,** Heat map displaying the elevation of FAO-related proteins in the FMD group, accompanied by the downregulation of IgA production related genes. **F–H,** The expression of CPT1A in B cells cultured for 5 days *in vitro* was detected using qPCR, FC, and Western blotting. **I–K,** After the addition of etomoxir, an irreversible inhibitor of CPT1A, or C75, an activator of CPT1A, the expression of IgA *in vitro* was examined using ELISPOT and FC. Etomoxir and C75 were initially dissolved in DMSO and diluted in media to a final DMSO concentration of 0.1%, while the control was supplemented with equal amounts of DMSO. Data are shown as means± SEM. ns, not significant; *, $P < 0.05$; **, $P < 0.01$; ***, $P < 0.001$; ****, $P < 0.0001$. CON, control; Eto, etomoxir. (**I,** Created with BioRender.com.)

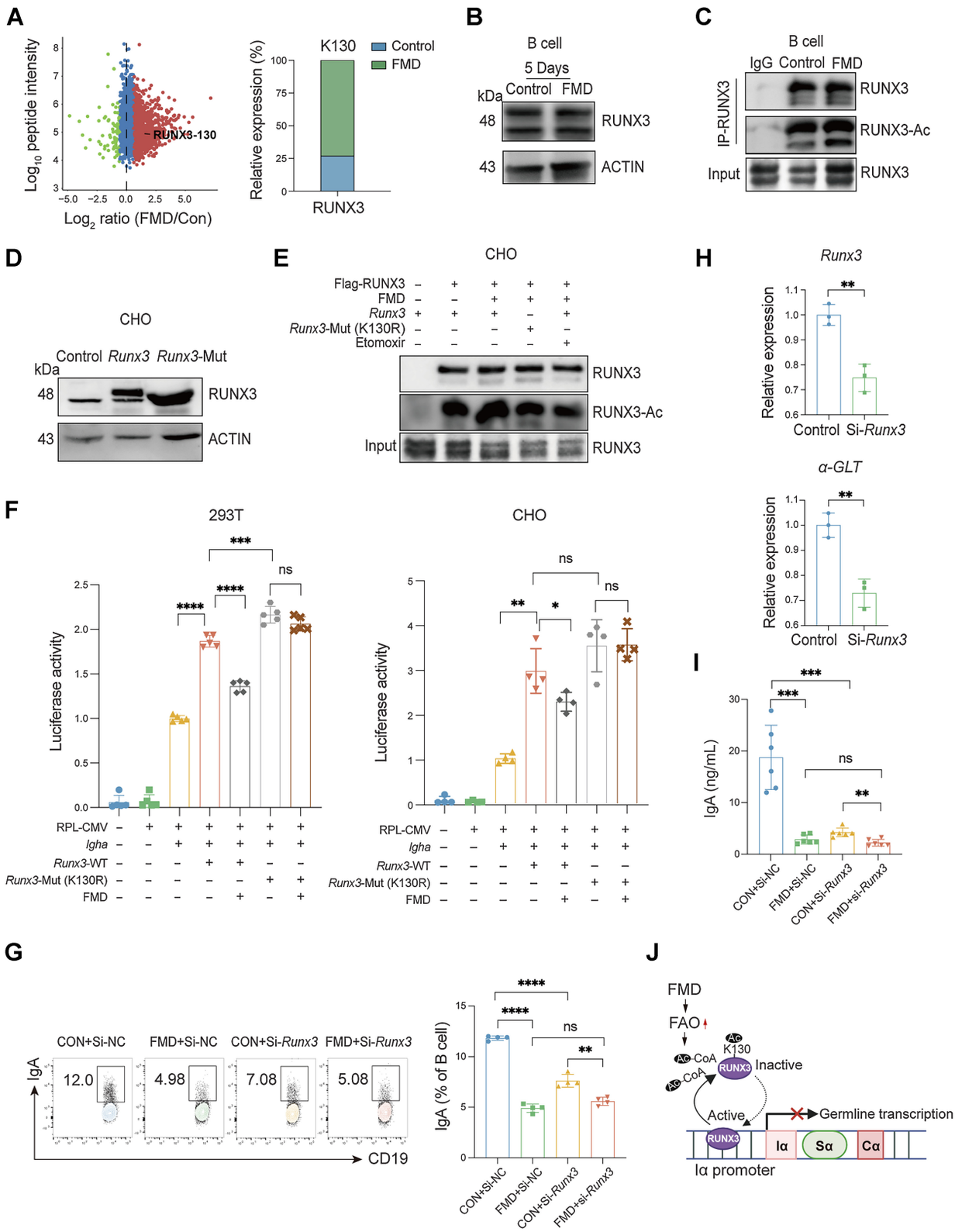
A
Log10 peptide intensity
Log2 ratio (FMD/Con)
RUNX3-130
Relative expression (%)
K130
Control
FMD
RUNX3
B
B cell
5 Days
kDa
Control FMD
48
RUNX3
43
ACTIN
C
B cell
IgG Control FMD
IP-RUNX3
RUNX3
RUNX3-Ac
Input
RUNX3
D
CHO
Control Runx3 Runx3-Mut
kDa
48
RUNX3
43
ACTIN
E
CHO
Flag-RUNX3
FMD
Runx3
Runx3-Mut (K130R)
Etomoxir
RUNX3
RUNX3-Ac
Input
RUNX3
H
Runx3
Relative expression
Control Si-Runx3
α-GLT
Relative expression
Control Si-Runx3
F
293T
CHO
Luciferase activity
RPL-CMV
Igha
Runx3-WT
Runx3-Mut (K130R)
FMD
I
IgA (ng/mL)
CON+Si-NC
FMD+Si-NC
CON+Si-Runx3
FMD+si-Runx3
G
CON+Si-NC
FMD+Si-NC
CON+Si-Runx3
FMD+Si-Runx3
IgA
12.0
4.98
7.08
5.08
CD19
IgA (% of B cell)
CON+Si-NC
FMD+Si-NC
CON+Si-Runx3
FMD+si-Runx3
J
FMD
FAO
CoA
K130
RUNX3
Inactive
Active
Germline transcription
Iα
Sα
Cα
Iα promoter

IFNγ$^+$CD8$^+$ T cells and reduced the frequency of IgA$^+$ B and PD-1$^+$CD8$^+$ T cells (Supplementary Fig. S7A–S7C). Moreover, FC and immunofluorescence staining were used to investigate the impact of FMD on IgA$^+$ B cells and the relationship between IgA cell percentage and CPT1A expression in B cells in all patients (**Fig. 6E–G**). The results proved that the FMD-induced reduction of IgA$^+$ B cells is paralleled by an increase in CPT1A in the B cells of patients with colorectal cancer. In addition, a significant reduction in IgA secretion was found in post-FMD feces compared with that in pre-FMD feces (**Fig. 6H**). Interestingly, we found that the amount of IgA in the tumor homogenate of the FMD group decreased considerably, but serum IgA secretion was not significantly different (**Fig. 6I** and **J**). In addition, linear regression analysis showed significant correlation between IgA in the tumor homogenate and CPT1A in B cells, whereas correlation was not significant for serum IgA secretion and CPT1A in B cells (**Fig. 6K**). Together, these results indicate that FMD impedes IgA$^+$ B-cell expansion within the local tumor microenvironment (TME) in patients with colorectal cancer, which was associated with CPT1A expression in intratumoral B cells.

Discussion

Cyclic fasting or FMD, which not only regulates systemic metabolism but also enhances the sensitivity of chemotherapy and immunotherapy, has recently attracted much attention in tumor therapy. A potential immune-enhancing effect of FMD was found in studies combining FMD with tumor therapy; however, the key immune cells on which FMD is mainly dependent to exert antitumor effects are still poorly understood. This study revealed the changes in the colorectal cancer immune cell atlas following FMD treatment and found that FMD promoted antitumor immunity by inhibiting IgA$^+$ B cells in both murine and human colorectal cancer. Mechanistically, FMD boosts the acetylation modification of the IgA transcription factor RUNX3 by promoting FAO, thereby repressing B cell CSR to IgA.

A key outcome of previous studies was the identification of immune remodeling in response to fasting in the TME (1, 10–12). It has been shown that FMD, CR, and caloric restriction mimetics (CRM) activate cancer immunosurveillance by triggering T lymphocyte–mediated cytotoxicity, altering NK cell function, and possibly driving immunogenic cell death via autophagy (13, 14, 23). Preclinical studies have demonstrated that FMD, as an adjunct to various cancer therapies, potentially improves antitumor immunity. In drug-treated cancer studies, FMD activates hematopoietic stem cell regeneration and the accumulation of memory T cells in the bone marrow compartment, thereby reducing immunosuppression and boosting CD8$^+$ cytotoxicity (13, 24). Fasting may also produce beneficial antitumor effects by altering the abundance of peripheral immune cells, including monocytes and a subset of dendritic cells, and limiting the polarization of innate immune cells, such as tumor-associated macrophages (TAM) and myeloid-derived suppressor cells (MDSC; refs. 25–27). However, the mechanism by which FMD regulates the function and polarization of B cells in the TME remains unclear. Earlier studies on inflammatory diseases and infections suggest that fasting markedly decreases memory-like B cell subsets and may induce a shift towards the naïve B-cell compartment (28, 29). As this study showed, compared with *ad libitum* conditions, FMD markedly decreased IgA$^+$ B cells in the local TME. These IgA$^+$ B cells had high expression of PD-L1 and TGFβ1 and possessed immunosuppressive properties, which is consistent with previous findings (14, 15, 17). TGFβ can not only regulate adaptive immunity by directly boosting Treg expansion and by controlling effector T-cell function, but also similarly affect the innate immune system by inhibiting NK cells and driving the differentiation of innate immune cells to highly immunosuppressive MDSCs and TAM, thereby forming a negative immune regulatory network (30, 31). Moreover, PD-L1 can directly inhibit the cytotoxic function of CD8$^+$T cells and NK cells, resulting in loss of tumor immunosurveillance (32). Specifically, our data showed that FMD-stimulated CD8 effector function and tumor regression were reversed after adoptive transfer of IgA$^+$ B cells, demonstrating a key role of IgA$^+$ B cells in FMD treatment.

In addition, we found an interesting phenomenon that neutrophils obviously increased in *Iga*$^{-/-}$ mice compared with WT mice. Studies have reported that the plasticity of neutrophils is a double-edged sword (33, 34). In response to TME stimulation, neutrophils polarize into either antitumoral or pro-tumoral phenotype and show different functions. High levels of IgA can bind to Fcα receptors (FcαR) expressed on neutrophils, thereby blocking antibody-dependent cell cytotoxicity (ADCC) and antibody-dependent cell phagocytosis (ADCP) by neutrophils (35, 36). Moreover, IgA helps to convert neutrophils to immune suppressive PMN-MDSC (36, 37). It thus appears that neutrophils may become a potential antineoplastic mechanism of FMD, which needs to be further studied in the future. In the current study, B cells have been shown to predominate within the TME; we thus focus on the effect of FMD intervention on B cells.

Metabolic reprogramming shifts immune cell fate and response. Several studies have demonstrated that the differentiation and survival of GC B cells are highly dependent on the mTOR signaling pathway (38). Recently, Kei Haniuda and colleagues proved that the reprogramming of TCA cycle metabolism mediated by IL4 promotes the accumulation of αKG, which integrates epigenetic activation of the Bcl6 gene to induce differentiation of GC B cells (39). Nevertheless, GC B cells rely on FAO rather than glycolysis to stimulate proliferation (40). The metabolites of glycolysis were

Figure 5.

FAO-triggered RUNX3 acetylation is responsible for hindering IgA class switching. **A,** B cells were isolated from the spleen of WT mice and treated with control or FMD medium for 5 days in the presence of MC38 supernatants and IgA class switching condition, and proteomic quantification of Lys acetylation was obtained using mass spectrometry. Each sample was pooled with four mice. It was identified that K130 was the major acetylation site of RUNX3 and RUNX3 acetylation was increased in FMD group. **B** and **C,** These results as in **A** were confirmed using Western blotting and IP. **D** and **E,** The CHO cells were transiently transfected with the indicated plasmids (**D**), incubated in a control or FMD medium for 48 hours in the presence or absence of etomoxir (**E**). Cell lysates were immunoprecipitated and immunoblotted with the indicated antibodies. **F,** Effects of FAO-dependent acetylation of Runx3 on *Igha* transcriptional regulation were measured using luciferase assays in 293T and CHO cell lines. **G–I,** The splenic B cells of mice were purified and *si-Runx3* was electro-transfected to B cells (other groups were electro transfected with the negative control siRNA for contrast). All groups were subsequently stimulated by LPS, TGFβ, BAFF, anti-CD40, and anti-IgM with control or FMD medium for 5 days *in vitro*. The percentage of IgA$^+$ B cells was measured using FC (**G**), interference efficiency of *Runx3*-siRNA was detected using qPCR (**H**), and the IgA level in the culture supernatant was measured using ELISA (**I**). **J,** Cartoon depicts the increase in Runx3 acetylation and the decrease in Runx3-dependent transcriptional activity after FMD treatment. Data are shown as means± SEM. ns, not significant; *, $P < 0.05$; **, $P < 0.01$; ***, $P < 0.001$; ****, $P < 0.0001$.

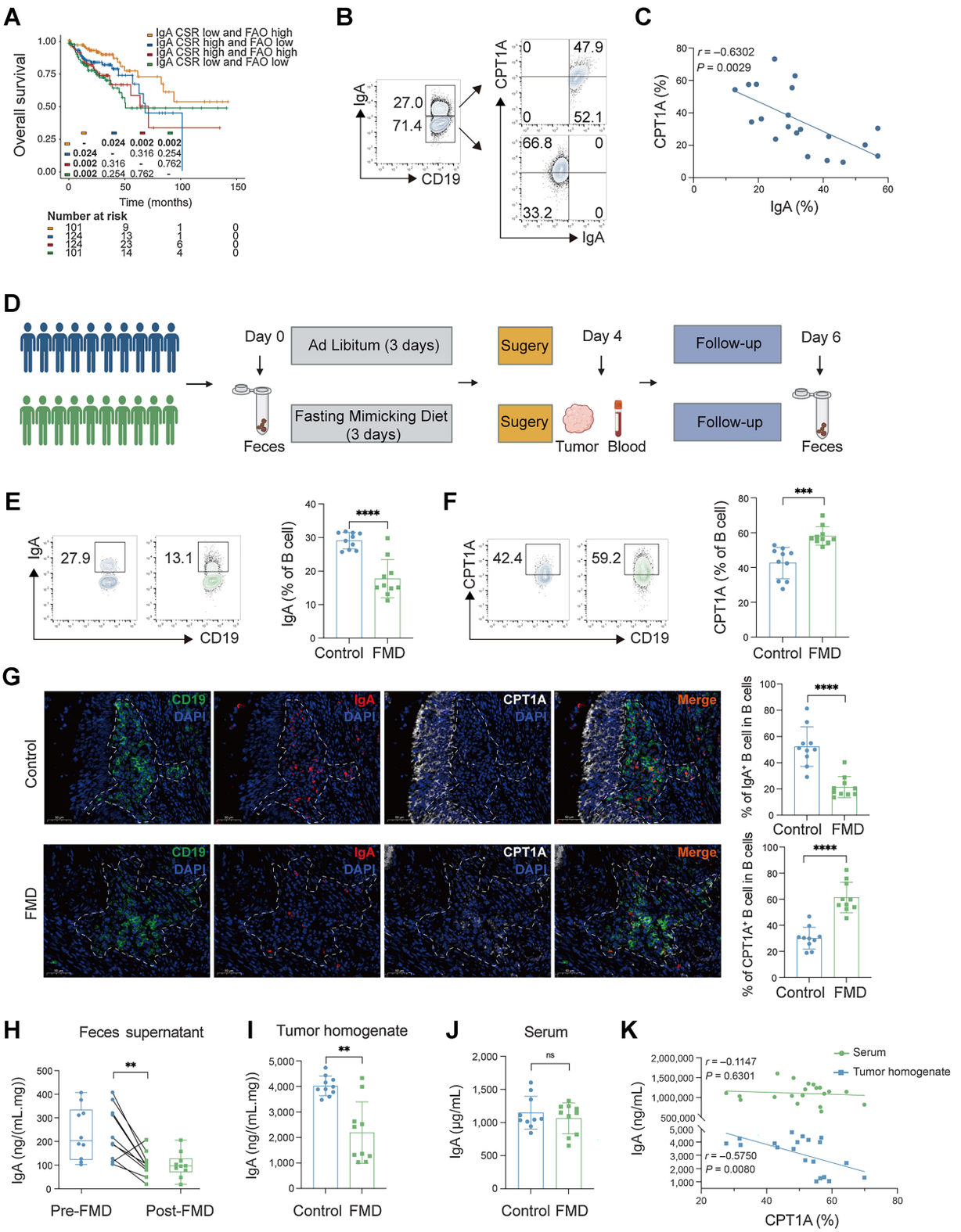
A
IgA CSR low and FAO high
IgA CSR high and FAO low
IgA CSR high and FAO high
IgA CSR low and FAO low
Overall survival
Time (months)
Number at risk
B
IgA
CD19
CPT1A
C
r = −0.6302
P = 0.0029
CPT1A (%)
IgA (%)
D
Day 0
Ad Libitum (3 days)
Fasting Mimicking Diet (3 days)
Feces
Sugery
Day 4
Tumor
Blood
Follow-up
Day 6
E
IgA (% of B cell)
Control
FMD
F
CPT1A (% of B cell)
G
CD19
DAPI
IgA
CPT1A
Merge
Control
FMD
% of IgA+ B cell in B cells
% of CPT1A+ B cell in B cells
H
Feces supernatant
IgA (ng/(mL.mg))
Pre-FMD
Post-FMD
I
Tumor homogenate
IgA (ng/(mL.mg))
J
Serum
IgA (μg/mL)
ns
K
Serum
Tumor homogenate
IgA (ng/mL)
r = −0.1147
P = 0.6301
r = −0.5750
P = 0.0080
CPT1A (%)

detected preferentially in IgA PCs compared with naïve B cells, suggesting that the shift to glycolysis-mediated energy metabolism is likely useful for the generation and production of IgA. Our team recently confirmed that the regulatory feature of LARS B cells is dependent on the regeneration of mitochondrial NAD^+ and oxidative metabolism (41). FMD could drive metabolic reprogramming in multiple cell types to improve disease prognosis (42, 43). However, it is largely unknown how FMD contributes to B-cell metabolism, and how alternations in metabolism impact IgA class switching. We proved that FMD impedes IgA class switching in a FAO dependent manner and that RUNX3 is involved. Inhibition of CPT1A, the rate-limiting enzyme in FAO, abrogates the reduction of IgA in the FMD group, while the activation of CPT1A markedly lowered the production of IgA, which implies a potential role for FAO in interfering IgA class switching.

As it is activated by induction of the Iα promoter, IgA CSR requires germline transcription (GLT) of Ig heavy chain constant α gene (Igα) and the expression of AID (21, 44). Overwhelming evidence indicated that TGFβ1 has a special role in IgA class switching. Several studies have demonstrated that Runx transcription factors act synergistically with Smad transcription factors in response to TGFβ family signaling (45). Moreover, RUNX3 and Smad2, 3 complex worked on the GLT promoter and enhanced transcriptional activity. Therefore, RUNX3 is believed to function as the activator of IgA CSR in B cells. In the current study, FAO metabolic pathways were more active after FMD intervention. Acetyl-CoA, the end products of FAO, occupies a crucial position within cell metabolic processes as a biosynthetic intermediate but also as a key determinant of protein acetylation (46). Therefore, the evidence for FMD-induced metabolic reprogramming prompted us to investigate acetylation, a posttranscriptional modification that is linked to metabolism and the availability of acetyl-CoA. It has been reported that CR and ketogenic diets elevate the levels of protein acetylation in the liver in mice (47, 48). However, CRMs enhanced the capacity to promote autophagy by reducing protein acetylation (49). Therefore, the impacts of fasting on acetylation might depend on tissue, cell type, and the precise protein species. Furthermore, no research has reported that FMD controls IgA CSR through acetylation modification of transcription factors. In the current study, we provide evidence that enhanced acetylation modification of RUNX3 driven by FMD resulted in the inhibition of IgA class switching.

The clinically FMD regimens are diverse, including various FMD duration (range: 2–5 days), different average daily caloric restriction (range 360–793.4 Kcal/day) and a wide variety of foods (3, 8, 13, 50–52). Our FMD regimen is based on one of previous researches, which has been reported to reshape systemic metabolism and antitumor immunity (3). Furthermore, in the current study, due to the requirement of a semi liquid diet for patients with colorectal cancer before surgery and the preoperative preparation time is usually relatively brief, we made some adjustments based on existing research. For instance, solid foods were replaced with semi liquid foods, and the FMD duration was changed to 3 days before surgery. Furthermore, our clinical FMD regimen was consistent with the mouse FMD protocol, which is a very-low-calorie, low-protein diet for 3 days to mimic a fasting-like state. We showed that a 3-day FMD cycle is sufficient to alter the local IgA of patients with colorectal cancer.

Accumulating clinical data have confirmed the beneficial effect of FMD alone or in combination with antitumor therapy. The first randomized controlled study suggested that FMD notably curtailed chemotherapy-induced DNA damage in T lymphocytes and reinforced the effects of neoadjuvant chemotherapy in patients with early breast cancer (8). A clinical trial of 101 patients with cancer confirmed that FMD was safe, feasible, and profoundly reshaped anticancer immunity (3). However, the effects of FMD on IgA levels in cancer have rarely been reported. Herein, clinical trial data showed that both IgA^+ B cells and IgA secretion were decreased in the local TME of patients with colorectal cancer undergoing FMD intervention. Consistently, previous studies have suggested that the elimination of IgA^+ B cells in tumors may be beneficial for boosting the efficacy of chemotherapy, immunity, radiation, and targeted therapy (14, 15).

In summary, FMD improves antitumor immunity by reducing B-cell class switching to IgA and involves a metabolic shift towards FAO. Owing to the tumor immunomodulatory effectiveness of targeting IgA^+ B cells and its therapeutic safety, FMD is of great promise as adjuvant therapy for colorectal cancer.

Authors' Disclosures

No disclosures were reported.

Authors' Contributions

Z. Zhong: Software, validation, investigation, methodology, writing–original draft, project administration. **H. Zhang:** Validation, methodology, writing–original draft. **K. Nan:** Methodology, writing–original draft. **J. Zhong:** Funding acquisition, validation, writing–review and editing. **Q. Wu:** Validation. **L. Lu:** Validation. **Y. Yue:** Validation. **Z. Zhang:** Validation. **M. Guo:** Validation. **Z. Wang:** Methodology. **J. Xia:** Software. **Y. Xing:** Methodology. **Y. Fu:** Methodology. **B. Yu:** Methodology. **W. Zhou:** Methodology. **X. Sun:** Methodology. **Y. Shen:** Validation, methodology. **W. Chen:** Funding acquisition, investigation. **J. Zhang:** Methodology. **J. Zhang:** Writing–review and editing. **D. Ma:** Writing–review and editing. **Y. Chu:** Writing–review and editing. **R. Liu:** Conceptualization, supervision, funding acquisition, writing–review and editing. **C. Miao:** Conceptualization, supervision, funding acquisition, writing–review and editing.

Figure 6.

FMD-induced IgA^+ B-cell deficiency is related to the enhanced FAO in patients with colorectal cancer. **A,** Survival analysis using 450 TCGA COAD samples by combining IgA CSR levels (*CD40L, TGFB1, SMAD2, SMAD3, SMAD4, RUNX3, CREB, ELF1, IL2, IL4, IL5, IL6, IL10, BAFF, TGFBR2, MYD88, TNFRSF13B, TRAF6, IKBKB, NFKB1*, and *AICDA*) with FAO levels (*ACADM*, *DLD*, *ECI1, CPT2, CPT1A, CPT1B, ECHS1, GCDH, GK, CRAT, CHKB, DECR1, ACSL5, HADH, ACADS, LIPE, SLC25A20, ACSL3, GPD2, ACSL4, HADHB, HADHA, ACADL, ACSL1*, and *ACADL*). **B** and **C,** The expression of IgA and CPT1A in B cells was determined using FC analysis in 20 patients with colorectal cancer. The correlation between IgA and CPT1A in B cells was identified. **D,** Time points of feces, blood and tumor tissue sample collection in the ChiCTR2200062524 trial. **E** and **F,** Frequencies of IgA and CPT1A in 20 patients with colorectal cancer in the ChiCTR2200062524 trial. **G,** Immunofluorescence staining evaluation of intratumor IgA and CPT1A in control and FMD tumor samples from two indicative patients (magnification, ×100). Bar plots showing results of immunofluorescence analyses of IgA and CPT1A in 20 patients with colorectal cancer who were enrolled in the ChiCTR2200062524 trial. **H–J,** The IgA level in tumor homogenate, serum, and feces supernatant was measured using ELISA. Feces samples collected before the initiation of the FMD are indicated as "Pre," whereas the samples collected on day 6 as shown in **D** are indicated as "Post." **K,** The correlation between IgA in serum and tumor homogenate and CPT1A in B cells was identified. Data are shown as means± SEM. ns, not significant; **, $P < 0.01$; ***, $P < 0.001$; ****, $P < 0.0001$. (**D,** Created with BioRender.com.)

Acknowledgments

The authors thank Dan Zhang, Xinwen Zhou from Institutes of Biomedical Science Fudan University and Yiwei Zhong from public technology platform, School of Basic Medical Sciences, Fudan University, for their assistance with mass cytometry, mass spectrum, and ELISPOT assay. The authors also acknowledge the support of BioRender.com for generating the figures.

This research was supported by the National Key Research and Development Program of China (NO. 2020YFC2008400, 2020YFC2008402), the National Natural Science Foundation of China (NO. 82072213, 82272192, 82281240019, 81972666, 81971868, 82172187, 81873948, 81871591, 81730045), Clinical Research Plan of SHDC (NO. SHDC2020CR1005A), Shanghai Leading Talent (NO. 2020–112), Program of Shanghai Academic Research Leader (NO. 20XD1423000, 22XD1420400), Intelligent Medical Service Project of Zhongshan Hospital (NO.2020ZHZS25), Nanchong City-School Cooperation Project (NO. 22SXQT0081).

The publication costs of this article were defrayed in part by the payment of publication fees. Therefore, and solely to indicate this fact, this article is hereby marked "advertisement" in accordance with 18 USC section 1734.

Note

Supplementary data for this article are available at Cancer Research Online (http://cancerres.aacrjournals.org/).

Received January 31, 2023; revised May 5, 2023; accepted August 15, 2023; published first August 21, 2023.

References

1. Nencioni A, Caffa I, Cortellino S, Longo VD. Fasting and cancer: molecular mechanisms and clinical application. Nat Rev Cancer 2018;18:707–19.
2. Turbitt WJ, Demark-Wahnefried W, Peterson CM, Norian LA. Targeting glucose metabolism to enhance immunotherapy: emerging evidence on intermittent fasting and calorie restriction mimetics. Front Immunol 2019;10:1402.
3. Vernieri C, Fucà G, Ligorio F, Huber V, Vingiani A, Iannelli F, et al. Fasting-mimicking diet is safe and reshapes metabolism and antitumor immunity in patients with cancer. Cancer Discov 2022;12:90–107.
4. Siegel RL, Miller KD, Fuchs HE, Jemal A. Cancer statistics, 2022. CA Cancer J Clin 2022;72:7–33.
5. Bianchi G, Martella R, Ravera S, Marini C, Capitanio S, Orengo A, et al. Fasting induces anti-Warburg effect that increases respiration but reduces ATP-synthesis to promote apoptosis in colon cancer models. Oncotarget 2015;6:11806–19.
6. Weng ML, Chen WK, Chen XY, Lu H, Sun ZR, Yu Q, et al. Fasting inhibits aerobic glycolysis and proliferation in colorectal cancer via the Fdft1-mediated AKT/mTOR/HIF1α pathway suppression. Nat Commun 2020;11:1869.
7. Di Tano M, Raucci F, Vernieri C, Caffa I, Buono R, Fanti M, et al. Synergistic effect of fasting-mimicking diet and vitamin C against KRAS mutated cancers. Nat Commun 2020;11:2332.
8. de Groot S, Lugtenberg RT, Cohen D, Welters MJP, Ehsan I, Vreeswijk MPG, et al. Fasting-mimicking diet as an adjunct to neoadjuvant chemotherapy for breast cancer in the multicenter randomized phase II DIRECT trial. Nat Commun 2020;11:3083.
9. Marinac CR, Nelson SH, Breen CI, Hartman SJ, Natarajan L, Pierce JP, et al. Prolonged nightly fasting and breast cancer prognosis. JAMA Oncol 2016;2:1049–55.
10. de Gruil N, Pijl H, van der Burg SH, Kroep JR. Short-term fasting synergizes with solid cancer therapy by boosting antitumor immunity. Cancers 2022;14:1390.
11. Pietrocola F, Pol J, Vacchelli E, Rao S, Enot DP, Baracco EE, et al. Caloric restriction mimetics enhance anticancer immunosurveillance. Cancer Cell 2016;30:147–60.
12. Ajona D, Ortiz-Espinosa S, Lozano T, Exposito F, Calvo A, Valencia K, et al. Short-term starvation reduces IGF-1 levels to sensitize lung tumors to PD-1 immune checkpoint blockade. Nat Cancer 2020;1:75–85.
13. Di Biase S, Lee C, Brandhorst S, Manes B, Buono R, Cheng CW, et al. Fasting-mimicking diet reduces HO-1 to promote T cell–mediated tumor cytotoxicity. Cancer Cell 2016;30:136–46.
14. Shalapour S, Font-Burgada J, Di Caro G, Zhong Z, Sanchez-Lopez E, Dhar D, et al. Immunosuppressive plasma cells impede T-cell–dependent immunogenic chemotherapy. Nature 2015;521:94–8.
15. Shalapour S, Lin XJ, Bastian IN, Brain J, Burt AD, Aksenov AA, et al. Inflammation-induced IgA+ cells dismantle anti-liver cancer immunity. Nature 2017;551:340–5.
16. Isaeva OI, Sharonov GV, Serebrovskaya EO, Turchaninova MA, Zaretsky AR, Shugay M, et al. Intratumoral immunoglobulin isotypes predict survival in lung adenocarcinoma subtypes. J Immunother Cancer 2019;7:279.
17. Liu R, Lu Z, Gu J, Liu J, Huang E, Liu X, et al. MicroRNAs 15A and 16–1 activate signaling pathways that mediate chemotaxis of immune regulatory B cells to colorectal tumors. Gastroenterology 2018;154:637–51.
18. Takahashi T, Morotomi M, Nomoto K. A novel mouse model of rectal cancer established by orthotopic implantation of colon cancer cells. Cancer Sci 2004;95:514–9.
19. Hite N, Klinger A, Hellmers L, Maresh GA, Miller PE, Zhang X, et al. An optimal orthotopic mouse model for human colorectal cancer primary tumor growth and spontaneous metastasis. Dis Colon Rectum 2018;61:698–705.
20. Neufert C, Becker C, Neurath MF. An inducible mouse model of colon carcinogenesis for the analysis of sporadic and inflammation-driven tumor progression. Nat Protoc 2007;2:1998–2004.
21. Cerutti A. The regulation of IgA class switching. Nat Rev Immunol 2008;8:421–34.
22. Jin J, Xiao Y, Chang JH, Yu J, Hu H, Starr R, et al. The kinase TBK1 controls IgA class switching by negatively regulating noncanonical NF-κB signaling. Nat Immunol 2012;13:1101–9.
23. Farazi M, Nguyen J, Goldufsky J, Linnane S, Lukaesko L, Weinberg AD, et al. Caloric restriction maintains OX40 agonist-mediated tumor immunity and CD4 T cell priming during aging. Cancer Immunol Immunother 2014;63:615–26.
24. Collins N, Han SJ, Enamorado M, Link VM, Huang B, Moseman EA, et al. The bone marrow protects and optimizes immunological memory during dietary restriction. Cell 2019;178:1088–101.
25. Taylor SR, Falcone JN, Cantley LC, Goncalves MD. Developing dietary interventions as therapy for cancer. Nat Rev Cancer 2022;22:452–66.
26. Fu C, Lu Y, Zhang Y, Yu M, Ma S, Lyu S. Intermittent fasting suppressed splenic CD205+ G-MDSC accumulation in a murine breast cancer model by attenuating cell trafficking and inducing apoptosis. Food Sci Nutr 2021;9:5517–26.
27. Sun P, Wang H, He Z, Chen X, Wu Q, Chen W, et al. Fasting inhibits colorectal cancer growth by reducing M2 polarization of tumor-associated macrophages. Oncotarget 2017;8:74649–60.
28. Sbierski-Kind J, Grenkowitz S, Schlickeiser S, Sandforth A, Friedrich M, Kunkel D, et al. Effects of caloric restriction on the gut microbiome are linked with immune senescence. Microbiome 2022;10:57.
29. Nagai M, Noguchi R, Takahashi D, Morikawa T, Koshida K, Komiyama S, et al. Fasting-refeeding impacts immune cell dynamics and mucosal immune responses. Cell 2019;178:1072–87.
30. Batlle E, Massagué J. Transforming growth factor-β signaling in immunity and cancer. Immunity 2019;50:924–40.
31. Kim BG, Malek E, Choi SH, Ignatz-Hoover JJ, Driscoll JJ. Novel therapies emerging in oncology to target the TGFβ pathway. J Hematol Oncol 2021;14:55.
32. Chen DS, Mellman I. Elements of cancer immunity and the cancer-immune set point. Nature 2017;541:321–30.
33. Giese MA, Hind LE, Huttenlocher A. Neutrophil plasticity in the tumor microenvironment. Blood 2019;133:2159–67.
34. Salcher S, Sturm G, Horvath L, Untergasser G, Kuempers C, Fotakis G, et al. High-resolution single-cell atlas reveals diversity and plasticity of tissue-resident neutrophils in non-small cell lung cancer. Cancer Cell 2022;40:1503–20.
35. Sharonov GV, Serebrovskaya EO, Yuzhakova DV, Britanova OV, Chudakov DM. B cells, plasma cells and antibody repertoires in the tumor microenvironment. Nat Rev Immunol 2020;20:294–307.

36. Zhong Z, Nan K, Weng M, Yue Y, Zhou W, Wang Z, et al. Pro- and anti-effects of immunoglobulin A–producing B cell in tumors and its triggers. Front Immunol 2021;12:765044.
37. Chen Z, Zhang G, Ren X, Yao Z, Zhou Q, Ren X, et al. Crosstalk between myeloid and B cells shapes the distinct microenvironments of primary and secondary liver cancer. Cancer Res 2023;CAN–23–0193.
38. Ersching J, Efeyan A, Mesin L, Jacobsen JT, Pasqual G, Grabiner BC, et al. Germinal center selection and affinity maturation require dynamic regulation of mTORC1 kinase. Immunity 2017;46:1045–58.
39. Haniuda K, Fukao S, Kitamura D. Metabolic reprogramming induces germinal center B cell differentiation through Bcl6 locus remodeling. Cell Rep 2020;33: 108333.
40. Weisel FJ, Mullett SJ, Elsner RA, Menk AV, Trivedi N, Luo W, et al. Germinal center B cells selectively oxidize fatty acids for energy while conducting minimal glycolysis. Nat Immunol 2020;21:331–42.
41. Wang Z, Lu Z, Lin S, Xia J, Zhong Z, Xie Z, et al. Leucine-tRNA-synthase-2–expressing B cells contribute to colorectal cancer immunoevasion. Immunity 2022;55:1067–81.
42. Mihaylova MM, Cheng CW, Cao AQ, Tripathi S, Mana MD, Bauer-Rowe KE, et al. Fasting activates fatty acid oxidation to enhance intestinal stem cell function during homeostasis and aging. Cell Stem Cell 2018;22:769–78.
43. Okawa T, Nagai M, Hase K. Dietary intervention impacts immune cell functions and dynamics by inducing metabolic rewiring. Front Immunol 2020;11:623989.
44. Zan H, Casali P. Epigenetics of peripheral B-cell differentiation and the antibody response. Front Immunol 2015;6:631.
45. Sugai M, Watanabe K, Nambu Y, Hayashi T, Shimizu A. Functions of runx in IgA class switch recombination. J Cell Biochem 2011;112: 409–14.
46. Choudhary C, Weinert BT, Nishida Y, Verdin E, Mann M. The growing landscape of lysine acetylation links metabolism and cell signaling. Nat Rev Mol Cell Biol 2014;15:536–50.
47. Sato S, Solanas G, Peixoto FO, Bee L, Symeonidi A, Schmidt MS, et al. Circadian reprogramming in the liver identifies metabolic pathways of aging. Cell 2017;170: 664–77.
48. Roberts MN, Wallace MA, Tomilov AA, Zhou Z, Marcotte GR, Tran D, et al. A ketogenic diet extends longevity and healthspan in adult mice. Cell Metab 2017; 26:539–46.
49. Madeo F, Carmona-Gutierrez D, Hofer SJ, Kroemer G. Caloric restriction mimetics against age-associated disease: targets, mechanisms, and therapeutic potential. Cell Metab 2019;29:592–610.
50. Brandhorst S, Choi IY, Wei M, Cheng CW, Sedrakyan S, Navarrete G, et al. A periodic diet that mimics fasting promotes multi-system regeneration, enhanced cognitive performance, and healthspan. Cell Metab 2015;22:86–99.
51. Valdemarin F, Caffa I, Persia A, Cremonini AL, Ferrando L, Tagliafico L, et al. Safety and feasibility of fasting-mimicking diet and effects on nutritional status and circulating metabolic and inflammatory factors in cancer patients undergoing active treatment. Cancers 2021;13:4013.
52. Caffa I, Spagnolo V, Vernieri C, Valdemarin F, Becherini P, Wei M, et al. Fasting-mimicking diet and hormone therapy induce breast cancer regression. Nature 2020;583:620–4.